Self-assembly of defined core-shell ellipsoidal particles at liquid interfaces

Jack Eatson [a,], Susann Müller [b,c,*], Benjamin Midtvedt [d], Antonio Ciarlo [d], Johannes Menath [c], Giuseppe Pesce [d,e], Andrew B. Schofield [b], Giovanni Volpe [d], Paul S. Clegg [b], Nicolas Vogel [c], D. Martin. A. Buzza [a], Marcel Rey [b,d,f]*

[a] Department of Physics and Astrophysics, G. W. Gray Centre for Advanced Materials, University of Hull, Hull HU6 7RX, United Kingdom;

[b] School of Physics and Astronomy, The University of Edinburgh, Peter Guthrie Tait Road, Edinburgh EH9 3FD, UK.

[c] Institute of Particle Technology (LFG), Friedrich-Alexander-Universität Erlangen-Nürnberg (FAU), Cauerstrasse 4, 91058 Erlangen, Germany

[d] Department of Physics, University of Gothenburg, SE-41296, Gothenburg, Sweden

[e] Fisica "Ettore Pancini", 9307 Università degli Studi di Napoli Federico II, Naples, Italy

[f] University of Münster, Institute of Physical Chemistry, Corrensstr. 28/30, 48149 Münster, Germany

Supplementary Figures:

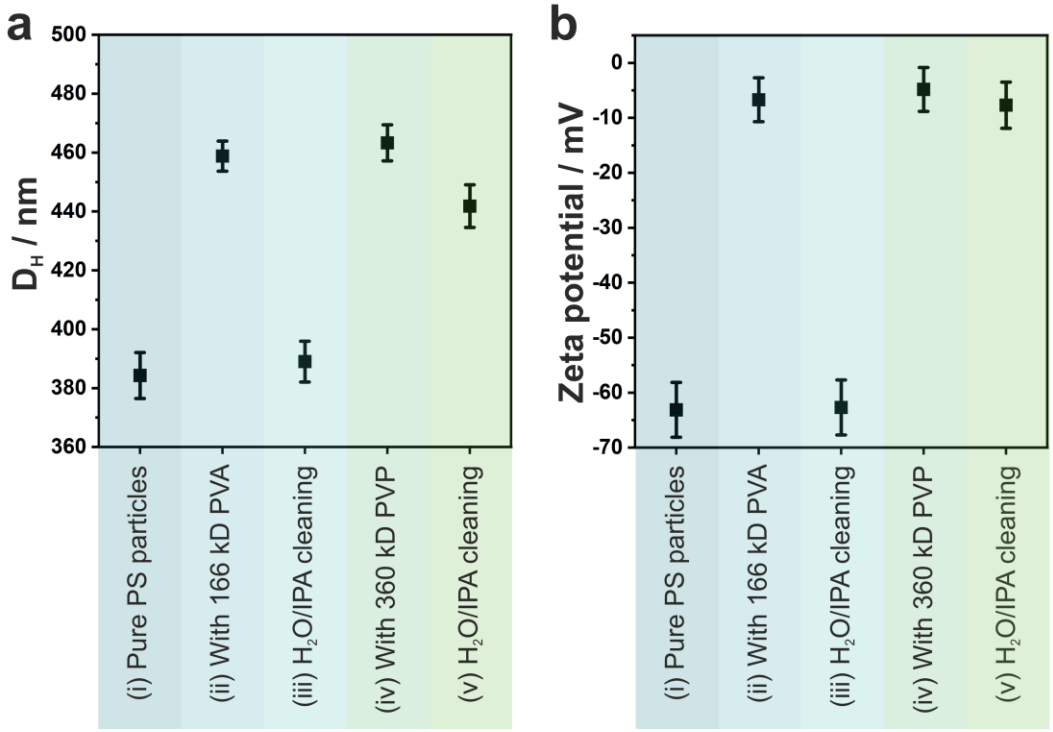

Fig. S1. a) Hydrodynamic diameter (D_H) and (b) zeta potential for the respective particle dispersions measured with dynamic light scattering. (i) Pure spherical polystyrene (PS) particles. (ii) After mixing PS particles with 166 kD PVA and subsequent removal of non-adsorbed PVA by centrifugation and redispersion in water, an increase in the D_H and decrease in zeta potential is observed, indicating the formation of a polymeric shell of physisorbed PVA. (iii) Washing these particles with an IPA/H_2O mixture removes the physisorbed PVA, as evidenced by the decrease in D_H and increase in zeta potential, returning to the value of the pure PS dispersion. (iv) When PS particles are mixed with 360 kDa PVP and the excess PVP is removed by centrifugation and redispersion in water, the hydrodynamic diameter increases and the zeta potential decreases, similar to the PVA case, indicating a physisorbed polymer shell. (v) After cleaning with the IPA/H_2O mixture, the D_H remains higher and the zeta potential lower than that of the pure PS particles, suggesting that the polymer shell at least partially persists even after washing.

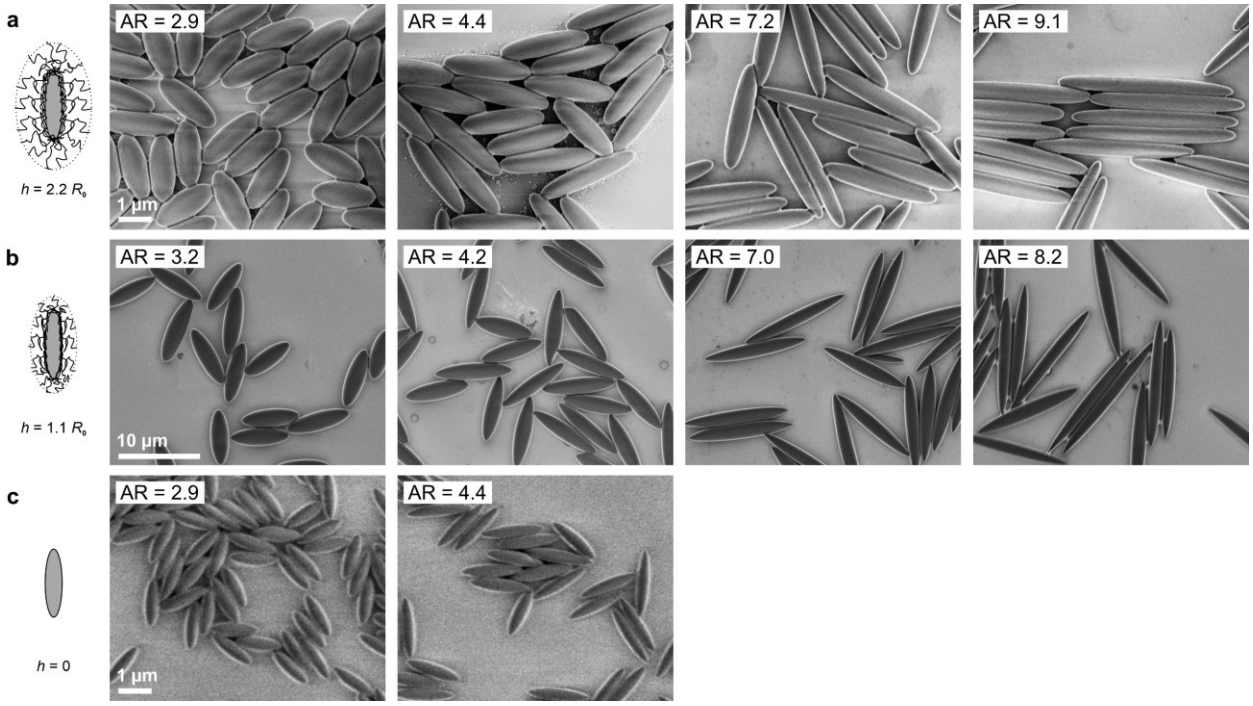

Fig. S2. Scanning electron microscopy (SEM) images of the ellipses used in Fig. 3. a) PS ellipsoidal particles containing a PVP shell. b) PMMA ellipsoidal particles with a PVP shell. c) Pure PS ellipsoidal particles with no shell.

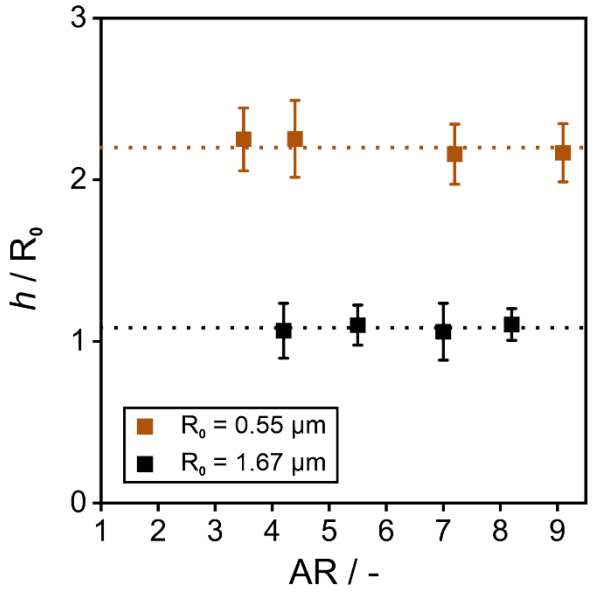

Fig. S3. Shell thickness *h* as a function of aspect ratio for PS-PVP particles (brown) and PMMA-PVP particles (black). The shell thickness *h* is determined by measuring the center-to-center distance for ellipsoidal particles in a side-to-side arrangement from optical microscopy images and subtracting the corresponding short-axis measurements obtained from SEM images.

1. Steric interaction between core-shell ellipsoidal particles

As discussed in the main paper, to model steric interactions between core-shell particles in our Monte Carlo (MC) simulations, we assume the shells are impenetrable and treat the core-shell particles at liquid interfaces as hard ellipses with long and short axis lengths of $a' = a + h$ and $b' = b + h$ respectively, where h is the experimentally measured shell thickness, $a = R_0 \mathrm{AR}^{2/3}$, $b = R_0 \mathrm{AR}^{-1/3}$ are the long and short axis lengths of the ellipsoidal core respectively, R_0 is the radius of the original unstretched spherical core and $\mathrm{AR} = a/b$ is the aspect ratio of the final stretched ellipsoidal core. This approach for modelling steric repulsions requires us to know the contact separation σ_c between hard ellipses, which is given in the Berne-Pechukas model [1] by

$$\sigma_c(\hat{\boldsymbol{u}}_1, \hat{\boldsymbol{u}}_2, \hat{\boldsymbol{r}}) = \sigma_\perp \left(1 - \frac{1}{2}\left[\frac{(\hat{\boldsymbol{r}} \cdot \hat{\boldsymbol{u}}_1 + \hat{\boldsymbol{r}} \cdot \hat{\boldsymbol{u}}_2)^2}{1 + \chi \widehat{\hat{\boldsymbol{u}}_1 \cdot \hat{\boldsymbol{u}}_2}} + \frac{(\hat{\boldsymbol{r}} \cdot \hat{\boldsymbol{u}}_1 - \hat{\boldsymbol{r}} \cdot \hat{\boldsymbol{u}}_2)^2}{1 - \chi \widehat{\hat{\boldsymbol{u}}_1 \cdot \hat{\boldsymbol{u}}_2}}\right]\right)^{-1/2}. \qquad (S1)$$

where $\hat{\boldsymbol{u}}_1$, $\hat{\boldsymbol{u}}_2$ are the unit vectors along the long axis of the two interacting ellipsoids, $\hat{\boldsymbol{r}}$ is the unit vector along the line joining the particle centres,

$$\chi = \frac{\sigma_\parallel^2 - \sigma_\perp^2}{\sigma_\parallel^2 + \sigma_\perp^2}$$

and $\sigma_\parallel = 2(a + h)$, $\sigma_\perp = 2(b + h)$ are the length and width of the hard ellipse respectively. Note that for prolate ellipsoidal particles, the Berne-Perchukas model for σ_c is accurate to within 2%. [2]

2. Capillary interaction between core-shell ellipsoidal particles

As discussed in the main paper, we assume that the capillary interactions between the core-shell ellipsoidal particles are due to quadrupolar contact line undulations on the ellipsoidal cores and this interaction is a function of the centre-to-centre separation of the interacting ellipsoidal particles r_{12} and the azimuthal angle that the long axis of each particle makes to the centre-to-centre φ_1, φ_2 as shown in Fig. S4. In this section, we follow ref. [3] and calculate the capillary interaction energy between two ellipsoid cores $V(r_{12}, \varphi_1, \varphi_2)$ by treating the contact line undulations on the cores as capillary quadrupoles in elliptical coordinates.

Assuming particle-centred coordinate systems and that the x and y axis of the Cartesian coordinate system are aligned along the long and short axis of the ellipsoidal particles respectively in the interfacial plane, the elliptical coordinates (s, t) are related to the Cartesian coordinates (x, y) by the transformations

$$x = \alpha \cosh(s) \cos(t) \qquad (S2)$$

$$y = \alpha \sinh(s) \sin(t) \qquad (S3)$$

where s, t are analogous to radial and polar coordinates respectively in circular polar coordinates and α is a scale factor (with dimensions of length) that determines the eccentricity of the constant-s lines in the elliptical coordinate system. Following ref. [3], we assume that the projection of the contact line on the interfacial plane corresponds to the outline the ellipsoidal core projected on the interfacial plane is given by the ellipse $s = s_0$. Making these assumptions, one can show that

$$\alpha = b\sqrt{\mathrm{AR}^2 - 1} \qquad (S4)$$

$$s_0 = \tanh^{-1}(1/\mathrm{AR}). \qquad (S5)$$

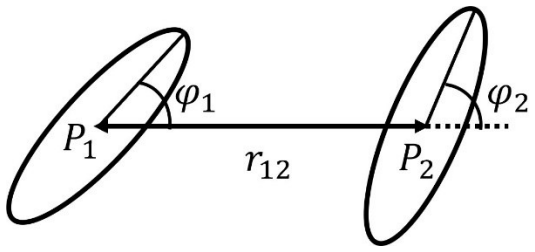

Fig. S4. The coordinates specifying the configuration of two interacting ellipsoidal particles at a liquid interface. The ellipses represent the projection of the contact line on each ellipsoidal particles on the interfacial plane while P_1, P_2 denote the centres of the two ellipsoidal particles on the interfacial plane.

A key parameter in calculating the capillary interaction is the position of the centre of particle 2 (P2) in a coordinate system where the centre of particle 1 (P1) is the origin. If we denote the position of P2 in Cartesian coordinates as (x', y'), from Fig. S4, we see that $x' = r_{12}\cos\varphi_1$, $y' = -r_{12}\sin\varphi_1$. Substituting this result into Equations (S2), (S3) and rearranging, we can write the position of P2 in elliptical coordinates (s^*, t^*) in terms of r_{12} and φ_1 as

$$s^* = \sinh^{-1}\left[\left\{\frac{1}{2}\left(\frac{r_{12}^2}{\alpha^2} - 1\right) + \frac{1}{2}\left[\left(\frac{r_{12}^2}{\alpha^2} - 1\right)^2 + \frac{4r_{12}^2\sin^2\varphi_1}{\alpha^2}\right]^{1/2}\right\}^{1/2}\right] \qquad (S6)$$

$$t^* = \sin^{-1}\left[\frac{-r_{12}\sin\varphi_1}{\alpha}\left\{\frac{1}{2}\left(\frac{r_{12}^2}{\alpha^2} - 1\right) + \frac{1}{2}\left[\left(\frac{r_{12}^2}{\alpha^2} - 1\right)^2 + \frac{4r_{12}^2\sin^2\varphi_1}{\alpha^2}\right]^{1/2}\right\}^{-1/2}\right]. \qquad (S7)$$

Finally, the interaction energy between the two elliptical quadrupoles is given by ref. [3]

$$V(r_{12}, \varphi_1, \varphi_2) = -2\gamma\pi\alpha^2 H_e \cosh(s_0)\sinh(s_0)\,[C'_{11}\cos(2\varphi_1 - 2\varphi_2) - C'_{21}\sin(2\varphi_1 - 2\varphi_2)] \qquad (S8)$$

where γ is the interfacial tension of the fluid interface, H_e is the amplitude of the elliptical quadrupolar and

$$C'_{11} = \frac{H_e e^{2s_0} e^{-2s^*}}{r_{12}^2 \cos^2\varphi_1 \,(\tanh^2 s^* - \tan^2 t^*)^2}\Bigg[4\cos(2t^*)(\tanh^2 s^* - \tan^2 t^*) - 8\sin(2t^*)\tan t^* \tanh s^* + 2(\tanh^2 s^* + \tan^2 t^*)(\cos(2t^*)\tanh s^* - \sin(2t^*)\tan t^*) - \frac{2\cos 2t^* \tanh s^*}{\cosh^2 s^*} - \frac{2\sin 2t^* \tan t^*}{\cos^2 t^*} + \frac{4(\cos(2t^*)\tanh s^* - \sin(2t^*)\tan t^*)}{\tanh^2 s^* + \tan^2 t^*}\left(\frac{\tanh^2 s^*}{\cosh^2 s^*} - \frac{\tan^2 t^*}{\cos^2 t^*}\right)\Bigg] \quad (S9)$$

$$C'_{21} = \frac{H_e e^{2s_0} e^{-2s^*}}{r_{12}^2 \cos^2\varphi_1 \,(\tan^2 t^* + \tanh^2 s^*)^2}\Bigg[4\sin(2t^*)(\tanh^2 s^* - \tan^2 t^*) + 8\cos(2t^*)\tan t^* \tanh s^* + 2(\tanh^2 s^* + \tan^2 t^*)(\sin(2t^*)\tanh s^* + \cos(2t^*)\tan t^*) - \frac{2\sin 2t^* \tanh s^*}{\cosh^2 s^*} + \frac{2\cos 2t^* \tan t^*}{\cos^2 t^*} + \frac{4(\sin(2t^*)\tanh s^* + \cos(2t^*)\tan t^*)}{\tanh^2 s^* + \tan^2 t^*}\left(\frac{\tanh^2 s^*}{\cosh^2 s^*} - \frac{\tan^2 t^*}{\cos^2 t^*}\right)\Bigg] \quad (S10)$$

where s^*, t^* are given by Equations (S6), (S7).

Note that in Equations (S8) – (S10), we have corrected some typographical errors in the corresponding equations in ref. [3]. Specifically, in Equation (S8), there is a minus between the two terms inside the square bracket (not a plus as shown in ref. [3]), while in Equations (S9), (S10), the denominator on the right hand side contains an extra factor of $\cos^2\varphi_1$ (which is missing in ref. [3]). Note also that, in spite of this extra factor, C'_{11}, C'_{21} do not diverge for $\varphi_1 \longrightarrow \pm\pi/2$ but tend towards finite limiting values. To avoid any numerical instabilities in our calculations, we therefore set C'_{11}, C'_{21} to be equal to these limiting values for φ_1 very close to $\pm\pi/2$.

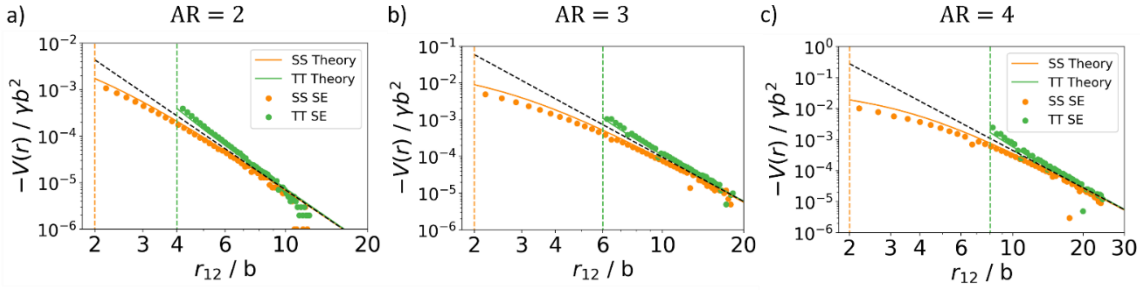

Fig. S5. Comparison of elliptical quadrupole model with Surface Evolver simulations for the capillary interaction energy as a function of centre-to-centre separation r_{12} for ellipsoidal particles with no shells and contact angle $\theta_w = 40°$ with aspect ratio (a) AR = 2; (b) AR = 3; (c) AR = 4. Note that in all cases we plot $-V$ in the vertical axis. We compare theory (solid lines) to simulations (data points) for ellipsoidal particles in the side-to-side configuration (red) and tip-to-tip configuration (blue). The red and blue vertical dashed lines represent the contact separation for the side-to-side and tip-to-tip configuration respectively while the dashed black line represents the quadrupolar power law. The values of the fitting parameter H_e used to fit theory to simulation for the different AR are given in Table S1.

In Fig. S5a,b,c, we compare our theoretical model, i.e., Equations (S6)-(S10), with Surface Evolver simulations for the interaction energy as a function of r_{12} for ellipsoidal particles with no shells and contact angle $\theta_w = 40°$ which have aspect ratios AR = 2,3,4 respectively. Specifically, we compare theory (solid lines) to simulations (data points) for ellipsoidal particles in the side-to-side (orange) and tip-to-tip configuration (green). We use H_e as a fitting parameter to fit the theory to the simulation data and the fitted values of H_e for the different AR are given in Table S1. We see that the theoretical model captures the key features of the numerical data almost quantitatively, including the far-field quadrupolar scaling of $V \sim -1/r_{12}^4$ (dashed black lines) and the near-field deviations from this scaling. The fitted values of H_e also agree with the amplitude of contact line undulations H_0 calculated directly from Surface Evolver simulations of isolated ellipsoidal particles to within a factor of around 2, where we define the amplitude to be $H_0 = (z_{max} - z_{min})/2$, i.e., half the difference in the maximum height z_{max} and minimum height z_{min} of the contact line (see Table S1). The good agreement between theory and simulations in Fig. S5 and Table S1 confirms that modelling the contact line undulations on the ellipsoid cores as elliptical quadrupoles is a good approximation.

As discussed in the main paper, the importance of capillary interactions relative to the thermal energy is characterized by the normalized temperature $T^* = k_B T/\gamma H_e^2$. In Table S1, we list the values of T^* for ellipsoidal particles with AR = 2,3,4 where we assume that $R_0 = 0.55\ \mu$m, $T =$ 300 K and $\gamma = 70$ mN·m^{-1}. We see that in all cases $T^* \ll 1$ and that T^* decreases with increasing AR. Since all the experimental ellipsoidal particles have AR > 2.5 and T^* will be lower for ellipsoidal particles with larger R_0 (since H_e is proportional to R_0), we conclude that all experimental systems we are studying in this paper are in the low temperature regime where $T^* \ll 1$.

Table S1: The amplitude of quadrupolar contact line undulations for ellipsoidal particles with $\theta_w = 40°$ and different aspect ratios AR obtained from fitting the elliptical quadrupole model to the Surface Evolver simulation data in Fig. S5 (H_e) and calculated directly from Surface Evolver simulations of isolated ellipsoidal particles ($H_0 = (z_{max} - z_{min})/2$, where z_{max}, z_{min} are the maximum and minimum heights respectively of the contact line). We also list the normalized temperature $T^* = k_B T/\gamma H_e^2$ for the ellipsoidal particles assuming $R_0 = 0.55$ μm, $T = 300$ K and $\gamma = 70$ mN·m^{-1}.

Aspect Ratio AR	H_e	H_0	T^*
2	$0.0205b$	$0.0506b$	7.4×10^{-4}
3	$0.0445b$	$0.0878b$	2.1×10^{-4}
4	$0.0690b$	$0.115b$	1.0×10^{-4}

References

[1] B.J. Berne, Philip Pechukas, Gaussian model potentials for molecular interactions, J Chem Phys 56 (1972) 4213–4216. https://doi.org/10.1063/1.1677837.

[2] F.D.J. Guevara-Rodríguez, G. Odriozola, Hard ellipsoids: Analytically approaching the exact overlap distance, J Chem Phys 135 (2011).

[3] E.P. Lewandowski, M. Cavallaro, L. Botto, J.C. Bernate, V. Garbin, K.J. Stebe, Orientation and self-assembly of cylindrical particles by anisotropic capillary interactions, Langmuir 26 (2010) 15142–15154. https://doi.org/10.1021/la1012632.